Vol. 2 • No. 5 • May • 2012

www.advenergymat.de

ADVANCED ENERGY MATERIALS

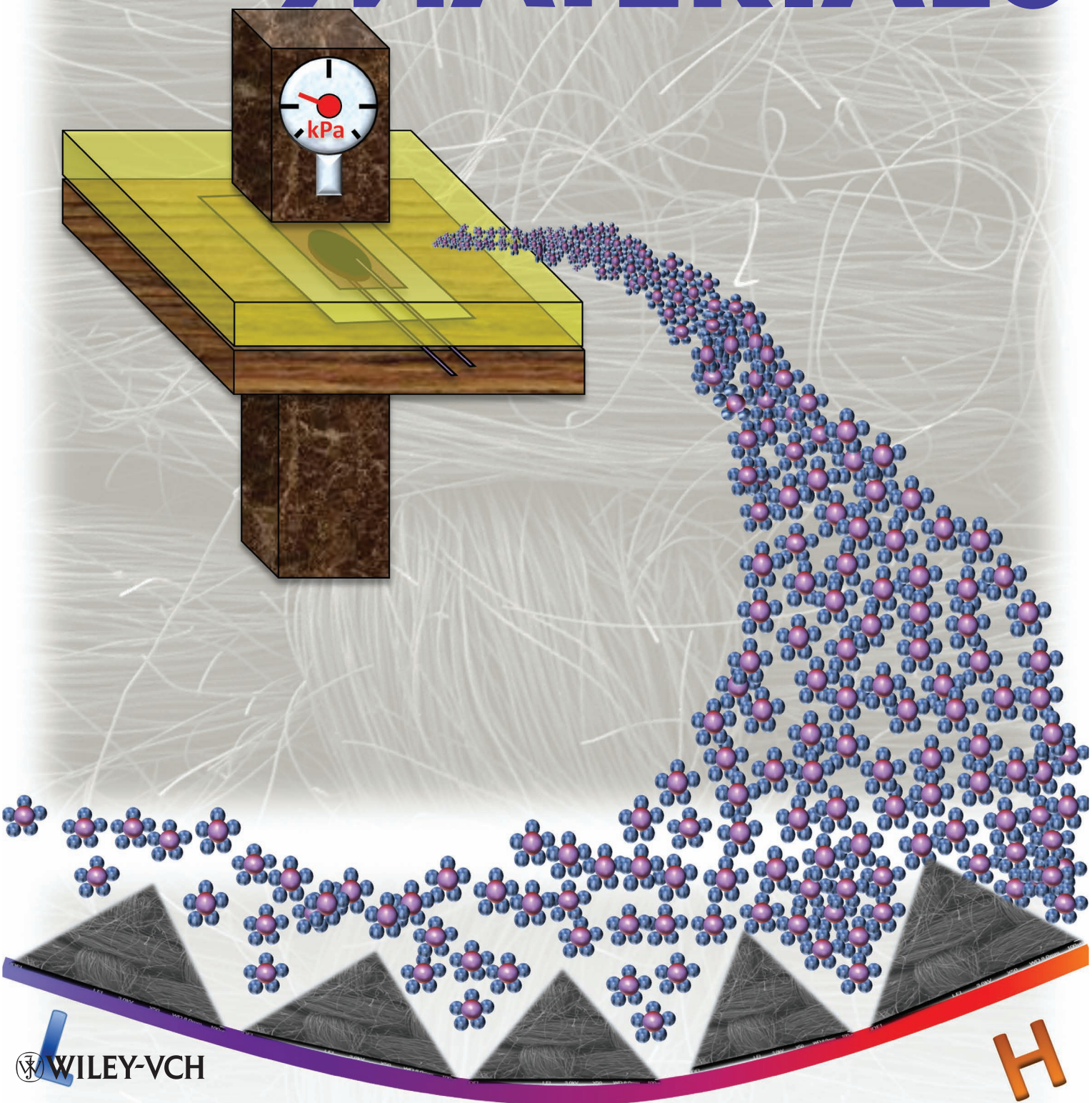

WILEY-VCH

FULL PAPER

Tailoring Electrode/Electrolyte Interfacial Properties in Flexible Supercapacitors by Applying Pressure

*Charan Masarapu, Lian-Ping Wang, Xin Li, and Bingqing Wei**

Electrode/electrolyte interfacial properties of flexible supercapacitors assembled with nanostructured activated carbon fabric (ACF) electrodes can be tailored by applying a pressure and tuning electrolyte ion size relative to electrode pore size. Experimental results reveal that increasing pressure between the supercapacitor electrodes can significantly improve capacitive performance. The ratio of solvated ion size in the electrolyte to the pore size on the electrodes determines the minimum pressure necessary to achieve an optimum performance. For a specific electrode material, this minimum pressure for optimum performance is primarily governed by the size of the larger solvated ions (either the anions or cations), and is lower (~689 KPa) when the ratio of the solvated ion size to the pore size is higher than 0.6, and is higher (at least 1379 KPa) when the ratio is lower than 0.6. An analytical model capable of predicting the experimental performance data has been developed. These results together provide a fundamental understanding of pressure dependence of electrode/electrolyte interfacial properties and pave the way for practical applications of flexible supercapacitors.

1. Introduction

Flexible electronic technology[1–4] has received increasing attention in the last two decades and rapid progress is being made most recently to realize several innovative devices such as flexible displays,[5] electronic paper,[6] functional electronic eyes,[7] and a cardiac electrophysiology mapping system.[8] To have an independent flexible electronic system, a flexible energy-storage device to provide power is indispensable. Recent publications have reported flexible supercapacitors with electrodes made of metal oxides, carbons, and composite materials.[9–14] These types of supercapacitors can have numerous applications in wearable electronics, smart cards, lightweight portable electronics, and several other day-to-day devices.

It is impossible for a thin-film supercapacitor embedded in a flexible plastic or elastic casing to avoid mechanical deformation such as stretching, bending, twisting, and compressing, where it encounters a variation in the pressure across its electrodes, depending on the way the device is used. For example, a supercapacitor in a device such as a smart credit card might be subjected to the enormous pressure of a human body when kept in the back pants pocket. These kinds of variations in the pressure between the electrodes affect the performance of the capacitor as they might change the contact resistance between the electrode and current collector, vary electrode/electrolyte interfacial properties, and cause deformations in the electrode materials. However, a fundamental understanding of this pressure effect between the two electrodes on the performance of a supercapacitor has not been tackled.

Research has already shown a strong correlation between electrode pore size and electrolyte ion size in supercapacitors.[15–18] Using linear-sweep voltammetry, Soffer et al. in the late seventies, observed adsorption of ions from solution into ultra-microporous carbon-fiber electrodes with pores much smaller than 1 nm.[15] In other recent works, the relation between electrolyte ion size and electrode pore size for optimum supercapacitor performance has been examined by different groups.[16–18] Until now, however, the dependence of pressure on the ion size in the electrolyte and the pore size of the electrode material has not been addressed in the literature. Fundamental understanding of the pressure-dependence of electrode/electrolyte interfacial properties in order to obtain the best electrochemical performance is crucial for thin-film and/or flexible supercapacitor devices, increasingly flexible/stretchable electronics, and for minimizing the required packaging resources as well.

Here, we report on the effect of pressure on the performance of thin-film flexible supercapacitors laminated in plastic pouches with nanostructured activated carbon fabric (ACF) electrodes in a variety of 1 M aqueous electrolyte solutions with salts of different cation and anion sizes. The pore size in the ACF electrodes is mostly distributed at 10 Å within the micropore region based on N_2 adsorption isotherm analysis (see Supporting Information (SI), Figure S1 for details). With its continuous fabric structure and uniform pore-size distribution, ACF provides a reliable foundation to investigate the ion size effects from the electrolyte under the application of pressure. A quantitative model describing the interdependence of the applied pressure between the electrodes and the ratio of solvated ion size of the electrolyte to the pore size of the electrode is presented, which closely matches the experimental results. A fundamental understanding of the pressure

Dr. C. Masarapu, Prof. L.-P. Wang, X. Li, Prof. B. Q. Wei
Department of Mechanical Engineering
University of Delaware
Newark, DE 19716, USA
E-mail: weib@udel.edu

DOI: 10.1002/aenm.201100529

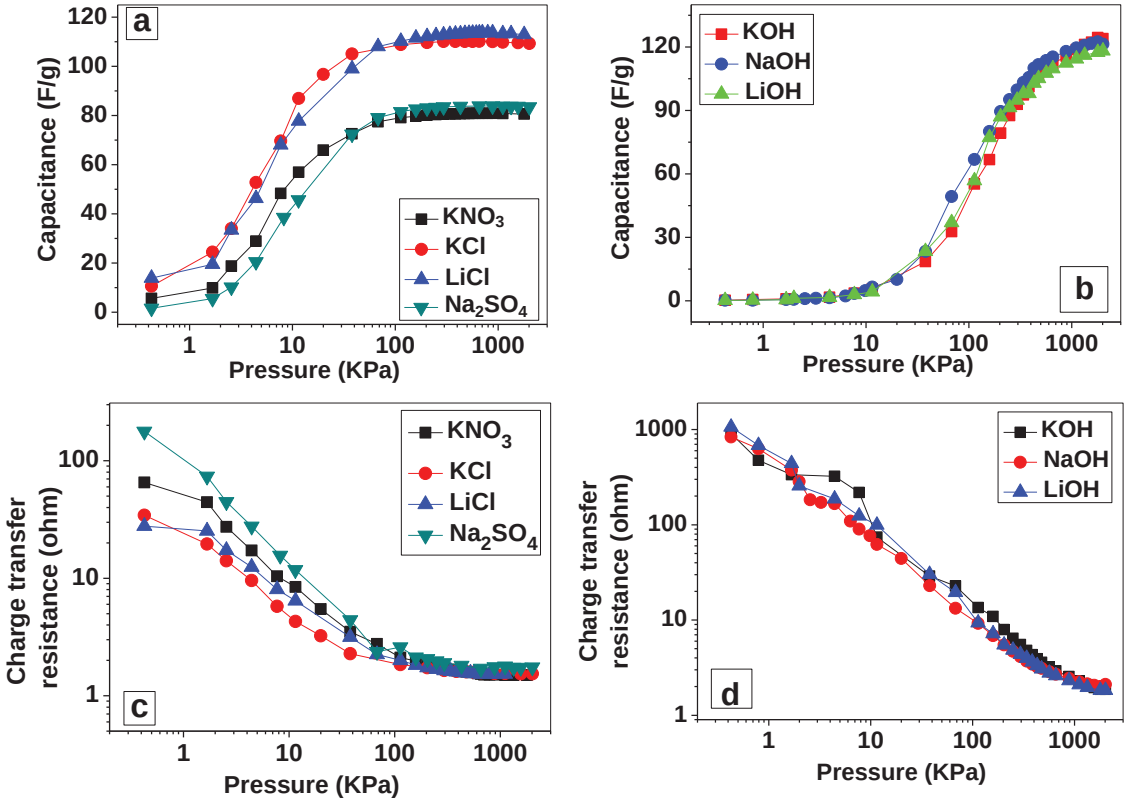

Figure 1. Supercapacitor performance with respect to the applied pressure. Variation of the capacitance of the supercapacitors assembled with ACF electrodes and the electrolytes a) KCl, KNO_3, LiCl, and Na_2SO_4, and the electrolytes b) LiOH, NaOH, and KOH. Variation of the charge-transfer resistance of the supercapacitors assembled with ACF electrodes and the electrolytes c) KCl, KNO_3, LiCl, and Na_2SO_4, and the electrolytes d) LiOH, NaOH, and KOH.

effect will allow us to tailor the electrode/electrolyte interfacial properties and allow deeper insights into the dependence of ion size and pore size on the applied pressure and optimum pressure requirements for the best supercapacitor performance.

2. Results

Variation of the capacitance obtained from cyclic voltammetry (CV) at 10 mV s^{-1} and the charge-transfer resistance obtained from electrochemical impedance spectroscopy (EIS) of all the capacitors with applied pressure were evaluated (see SI for details) and complement each other well (**Figure 1**). At very low applied pressures, the initial charge-transfer resistances are high (Figure 1c,d) and thus the capacitances obtained are very low (Figure 1a,b) in all the supercapacitors. As the charge-transfer resistance decreased with the gradual increase in the pressure, the capacitance increased in all cases. For the supercapacitors with electrolytes KCl, KNO_3, LiCl, and Na_2SO_4, the charge-transfer resistance reached a saturation at an applied pressure of about 414 kPa (Figure 1c), which corresponded to a capacitance saturation (Figure 1a). However, the charge-transfer resistances of the supercapacitors with electrolytes KOH, NaOH, and LiOH kept on decreasing with the addition of pressure up to 2068 kPa, supporting a continuous increase in the capacitances (Figure 1b). These supercapacitors require pressures exceeding 2068 kPa for the capacitance values to saturate.

To simplify further discussion, the electrolytes are divided into two groups—Group A and Group B—based on the results obtained in Figure 1. All the electrolytes corresponding to the supercapacitors whose capacitance values became saturated below 689.5 kPa are categorized as Group A (KCl, LiCl, Na_2SO_4, and KNO_3). The remaining electrolytes are categorized as Group B (NaOH, KOH, and LiOH). The CVs and EIS spectra of two supercapacitors assembled with the electrolytes containing the salts LiCl from Group A (**Figure 2**a,b) and LiOH from Group B (Figure 2c,d) show the typical difference. For all the applied pressures above 414 kPa, the impedance and CVs of the supercapacitor with LiCl electrolyte have very negligible to no difference, while the impedance and CVs of supercapacitors with LiOH electrolyte vary with respect to the pressure up to 2068 kPa. In both capacitors, the values of the solution resistance did not differ significantly with the variation in pressure (Figure 2b,d), indicating that the solution resistance is not being affected by the pressure changes. A similar behavior was observed in all the supercapacitors assembled with electrolytes in both Group A and Group B. This is because the electrolyte resistance depends on factors such as temperature and ion concentration, but not on mechanical variations in the supercapacitor. As the pressure between the electrodes increased, the charge-transfer resistance decreased and the CVs acquired a regular, rectangular shape from a distorted shape, approaching ideal capacitive behavior.

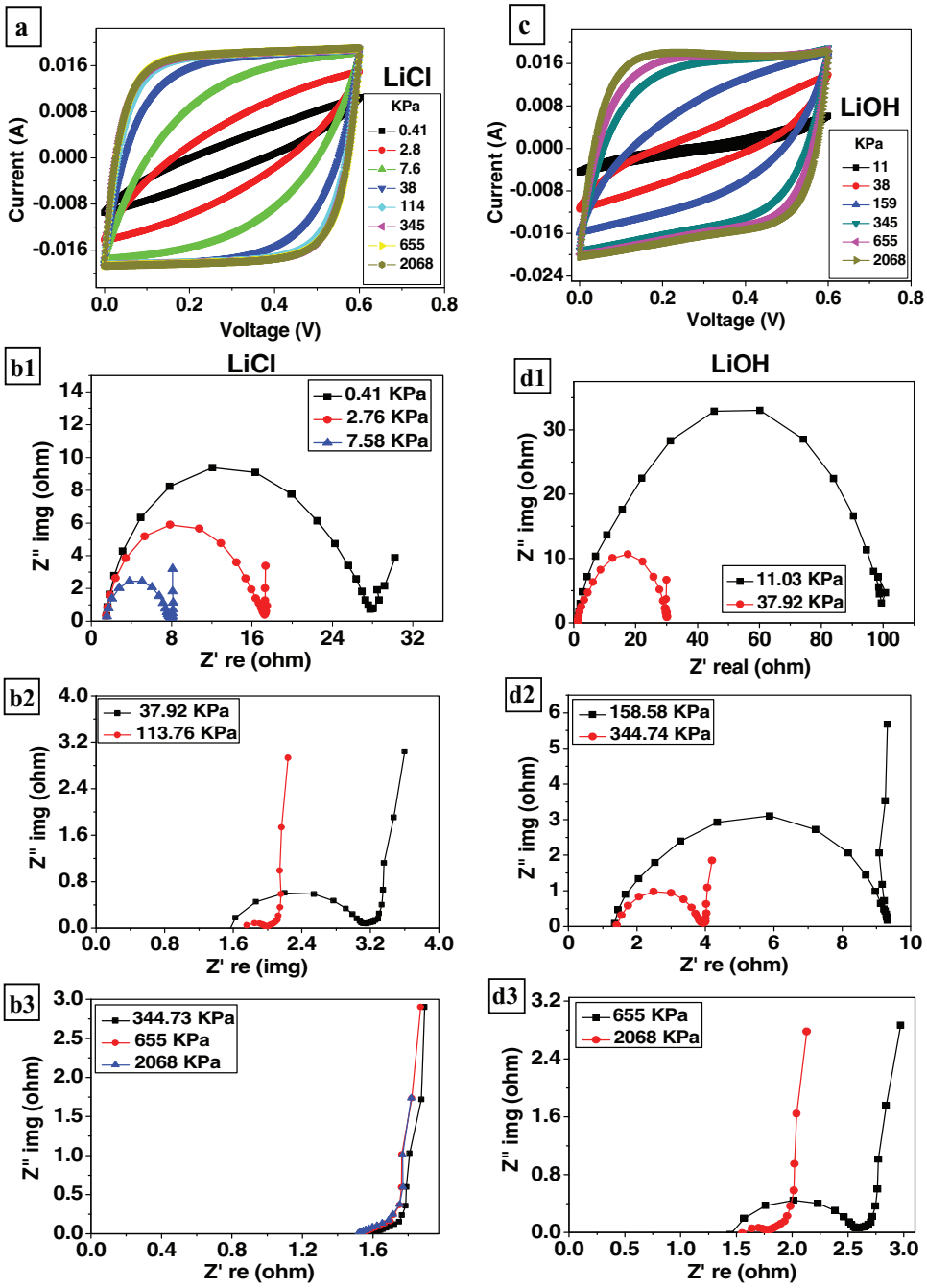

Figure 2. Behavior of the supercapacitors with electrolytes from Group A and Group B . Variation of the a) CVs and b) EIS spectra of the capacitor assembled with LiCl (Group A). Variation of the c) CVs and d) EIS spectra of the capacitor assembled with LiOH (Group B).

3. Discussion

3.1. Applied Pressure Governs the Pore Filling Efficiency in the Supercapacitor

The capacitance in a supercapacitor is governed by the availability of free ions near the electrode/electrolyte interface and the adsorption of these ions into the electrode pores for double-layer formation. The ions in an aqueous solution are generally present in their hydrated (solvated) forms and the size of the hydrated cation or anion depends on factors such as the concentration of the solution and the type of the salt being used. In the case of supercapacitor electrodes with smaller pore sizes (such as less than 1 nm), much of the capacitance is contributed by the desolvated ions adsorbed into the pores of the electrode[18,19] instead of solvated ions that are normally comparable to the pore size. Based on the literature,[20–25] the approximate sizes of hydrated cations and anions were estimated (SI, Table S1), where Li^+ is the smallest of all the ions and SO_4^{2-} is the largest ion in the current experiments. Thus, the

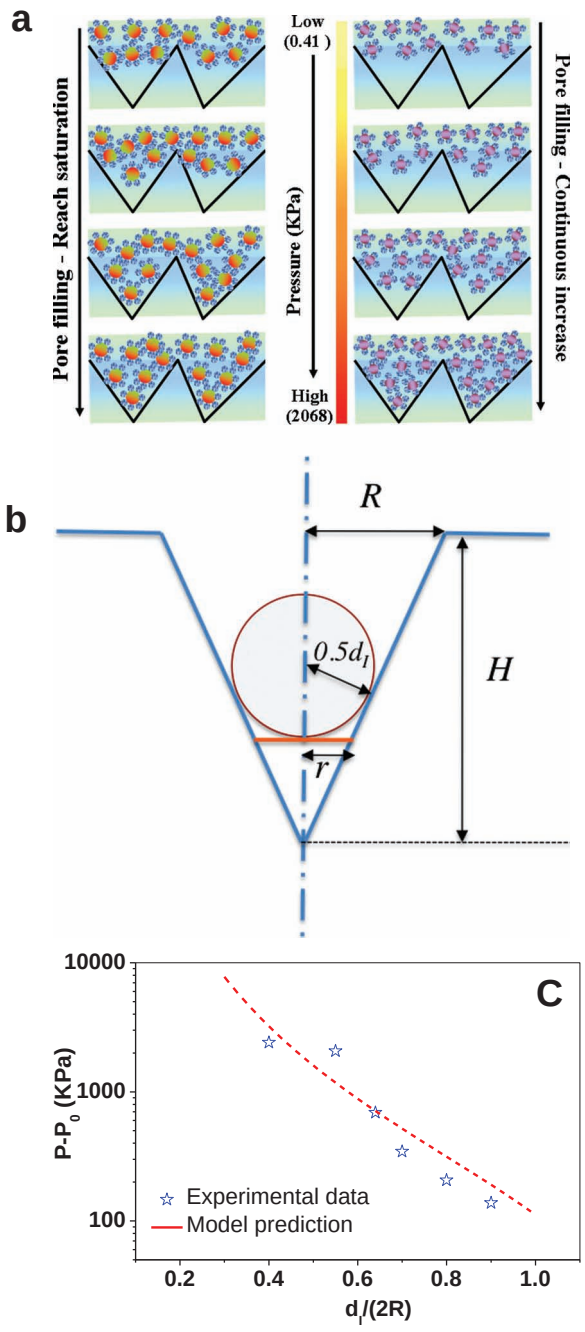

Figure 3. Generalization of the dependence of pressure on ion size and pore size. a) Schematic representation of the electrode/electrolyte interface of two different supercapacitors with an electrolyte from Group A (left side) and from Group B (right side). The wedge-shaped black lines represent the pores in the ACF electrodes. The circular dots represent the larger hydrated ions, either the cations or the anions (see SI, Figure S4) in the electrolyte. When the hydrated ions are much smaller compared to the pore size of the electrode (salts from Group A), the ions are increasingly forced into the pores all the way up to the applied pressure of 2068 kPa, causing the capacitance to continuously increase. In the case of larger hydrated ions compared to the pore size (salts from Group B), the pores are saturated, thus the capacitance saturates, at a lower applied pressure (left side). b) A sketch used to construct the model for the saturation pressure. c) Comparison between the measured saturation pressure and the modelled saturation pressure as a function of the ratio of ion size to pore size.

saturation or a continuous increase in the capacitance of a supercapacitor with increasing pressure can be explained by the pore-filling efficiency, based on the size of the ions in the electrolyte solution and the pore size of the electrode.

Since the scan rate of the CV influences the diffusion of the ions into the pores of the electrode, pressure measurements were done at different scan rates of 1 and 50 mV s^{-1} for two salts, LiCl (Group A) and KOH (Group B), and compared to the measurement done at 10 mV s^{-1} (SI, Figure S10). Decreasing the scan rate of the CV from 10 to 1 mV s^{-1} gave a higher capacitance at a given pressure but the trend in the variation of the capacitance with respect to pressure at both 1 and 50 mV s^{-1} remains the same as that obtained at 10 mV s^{-1}. For the capacitor with the salt LiCl, the capacitance saturates at a low pressure, while in the capacitor with the salt KOH the capacitance keeps increasing with increasing pressure at all scan rates.

The effect of pressure on the pore-filling efficiency of different-sized ions in the electrolyte can be shown in a schematic (**Figure 3**a). When there is no applied pressure or at a very low pressure, the electrolyte in the supercapacitor simply wets the ACF electrodes with the hydrated ions (SI, Figure S5), which are actually adsorbed onto the surface of the pores (Figure 3a) due to surface tension effects and the entrapped gases in the pores of the electrodes. When a voltage is applied between the electrodes, the double-layer formation is very weak as most of the surface area is devoid of ions. This scenario can explain the high charge-transfer resistance and the significantly distorted CVs from the ideal rectangular behavior with a very low applied pressure (Figure 2a,c). When the applied pressure between the electrodes increases gradually, the ions in the electrolyte solution are forced into the pores of the ACF electrodes to form a stable double layer when a voltage is applied. Increasing the pressure enhances the pore-filling efficiency (Figure 3), decreases the charge-transfer resistance (Figure 2b,d), and causes the CVs to gradually acquire an ideal rectangular shape (Figure 2a,c). As the pressure between the electrodes reaches a certain value, the electrolyte ions can no longer penetrate any deeper into the pores of the ACF electrodes, yielding a maximum capacitance that cannot be changed with any further pressure increase. Note that the pore-filling saturation with larger ions occurs at a lower pressure (left side of Figure 3a) than the electrolyte with smaller ions (right side of Figure 3a).

One interesting feature shown in Figure 2 can be explained based on the schematic in Figure 3a. In the impedance spectra of the supercapacitor with the Group B salt, the semicircle in the high-frequency region is present up to the applied pressure of 2068 kPa. However, the semicircle almost disappears at applied pressures higher than 345 kPa in the capacitor with the salt from Group A. The absence of the semicircle in the complex impedance plane implies a good conductivity of the ions in the pores of the electrode.[26] Since the hydrated ion size (salts in Group B) is much smaller compared to the pore size (~1 nm), more ions can be forced into the pores of the electrode with a higher applied pressure (right side of Figure 3a). For larger ions, however, a very limited number of ions can be pushed into the pores of the electrode (left side of Figure 3a). The presence of a large number of ions reduces their mobility in the pores and in turn, results in a reduction in conductivity when compared to that of hydrated ions whose sizes are comparable to the electrode pores.

To quantitatively demonstrate the relationship between the applied pressure, the obtained capacitance, and the ratio of the solvated ion size to pore size, an analytical model was developed based on a few reasonable assumptions (see SI for details). It follows the basic idea that the electrolyte ions will be pushed into the pores of the ACF as the pressure is increased, and so the capacitance is increased. It is assumed that, in the reference case of a flat interface covering the cone base (Figure 3b), the air pressure inside the cone is the same as the solution reference pressure, say P_0 (~1 atm or 101.3 kPa = 14.7 PSI). As the solution pressure is increased, the air–water interface is being pushed into the cone region. Since the air is trapped in the cone, the flow pressure has to overcome both capillary pressure and the trapped air pressure. The saturation guage pressure is size-dependent and is given as $P - P_0 = P_0\left[\left(\frac{2R}{d_1 f_c}\right)^3 - 1\right]$, where d_1 is the diameter of the ion size and the dimensionless geometric correction factor is $f_c\left(\frac{H}{R}\right) = \sqrt{1+\left(\frac{R}{H}\right)^2} - \frac{R}{H}$.

Figure 3c demonstrates the comparison between the measured saturation pressure and the model saturation pressure as a function of the ratio of ion size to pore size, verifying the simple analytical model.

3.2. Larger Solvated Ion Size Controls the Capacitance Saturation with Pressure

It can be noted from Figure 1 that the larger ion in the electrolyte, either the cation or the anion, solely controls the capacitance saturation with an applied pressure. This is evident from the fact that the capacitance of the supercapacitor with LiCl is saturating at an applied pressure of about 414 kPa, whereas the capacitance of the supercapacitor with LiOH is not saturating even at a pressure of 2068 kPa (Figure 2a,c). The two electrolytes have the same cation but different anions. Similar results were obtained for capacitors with the salts KCl and KOH (Figure 1). By paying close attention to the sizes of the solvated ions in SI, Table S1, an important difference can be noted between the electrolytes with salts of Group A and Group B. In each of the Group A salts, either the hydrated anion or cation is at least as large as the hydrated Cl^- ion. In the Group B salts, it can be observed that the hydrated anions and cations are all smaller than the hydrated Cl^- ion. The size of the hydrated Cl^- ion clearly highlights the difference between ions that saturate the capacitance within the 2068 kPa and ions that do not saturate the capacitance, even at 2068 kPa. To further support this finding, pressure measurements on supercapacitors with the salts KI (Group A) or KF (Group B) were performed (SI, Figure S6). The capacitance of the supercapacitor with KI saturated (the hydrated I^- ion is bigger than the hydrated Cl^- ion) whereas no saturation in the capacitance was observed in the capacitor with KF within 2068 kPa of applied pressure (hydrated F^- is smaller than hydrated Cl^-).

This experiment clearly presents the importance of applied pressure between the electrodes and its critical dependence on electrode pore size and ion size in the electrolyte in governing the capacitance of a supercapacitor. By considering this size exclusion effect with a larger ion size for a given pore size, we can analytically address the experimental phenomenon observed above. As shown in **Figure 4** (Figure 4a for small ions and Figure 4b for large ions), there are some unused spaces due to the finite-size effect, though a pore may still be filled effectively by more than one ion due to the 3D geometry. The pore behaves more like a flat surface for larger ions, implying earlier pressure saturation may occur. This may be modeled by introducing an empirical factor γ as follows;[27]

$$\text{Capacitance} = \begin{cases} \frac{C_1}{\beta_1 d_1^2}\left[1 - f + f\sqrt{1+\left(\frac{H}{R}\right)^2}\left(1-\left(\frac{P_0}{P}\right)^{\frac{2}{3}+\gamma}\right)\right], \\ \text{for } P \le P_0\left(\frac{2R}{d_1 f_c}\right)^3 \quad (1) \\ \frac{C_1}{\beta_1 d_1^2}\left[1 - f + f\sqrt{1+\left(\frac{H}{R}\right)^2}\left(1-\left(\frac{P_0}{P}\right)^{2+3\gamma}\right)\right], \\ \text{for } P \ge P_0\left(\frac{2R}{d_1 f_c}\right)^3 \quad (2) \end{cases}.$$

The above also incorporates the model for saturation pressure discussed before. Here, f is the percentage of flat surface on the ACF covered by the pores, β_1 is a geometric packing configuration parameter taking a value from 0.866 to 1, C_1 is a parameter used to convert the number density of ions per unit projected surface area to the capacitance,[27] γ is a model fitting parameter depending on the ratio d_I/R. The model results are based on $H/R = 4$, $f = 0.85$, $\beta_1 = 0.866$, and $R = 0.5$ nm; other case-dependent parameters are provided in the figure caption. The results from this empirical model are shown in Figure 4c–e, along with experimental data. The results show that the empirical model for the ion size effect quantitatively matches the experimental data well. This is quite good, considering that a large number of assumptions are made in the model and various viscous, chemical, and electrical effects are not explicitly treated.

The above experimental and theoretical results will have a significant impact on flexible/strechable supercapacitor assembly and packaging, as they provide a fundamental understanding of why it is necessary to choose a high-surface-area electrode material with a specific pore-size distribution and an electrolyte with suitable cation and anion sizes. The pressure between the electrodes plays a critical role, especially when supercapacitor assembly has to be done in a thin casing. This is required when capacitors are built from a flexible organic or elastic rubber material instead of the usual rigid coin-cell or prismatic-cell assembly. In addition, the previously observed variation in the capacitance of a flexible supercapacitor upon deformation can now be explained through the dependence of capacitance on the applied pressure between the electrodes. In a flexible supercapacitor, the stability of the electrode material is of the utmost importance in order to maintain normal performance under varying applied strain. In this regard, ACF electrodes are excellent materials for flexible supercapacitors and can withstand pressures as high as 2068 kPa while still retaining their capacitive performance with the repeated application of pressure (SI, Figure S9).

In summary, the pressure dependence of the performance of supercapacitors assembled with ACF electrodes has been demonstrated, in various 1 M aqueous electrolyte solutions with the salts LiOH, KOH, NaOH, LiCl, KCl, KNO_3, and Na_2SO_4. The size of the larger anions or cations in the electrolyte, relative to the pore size of the electrode, governs the capacitance saturation of supercapacitors at elevated

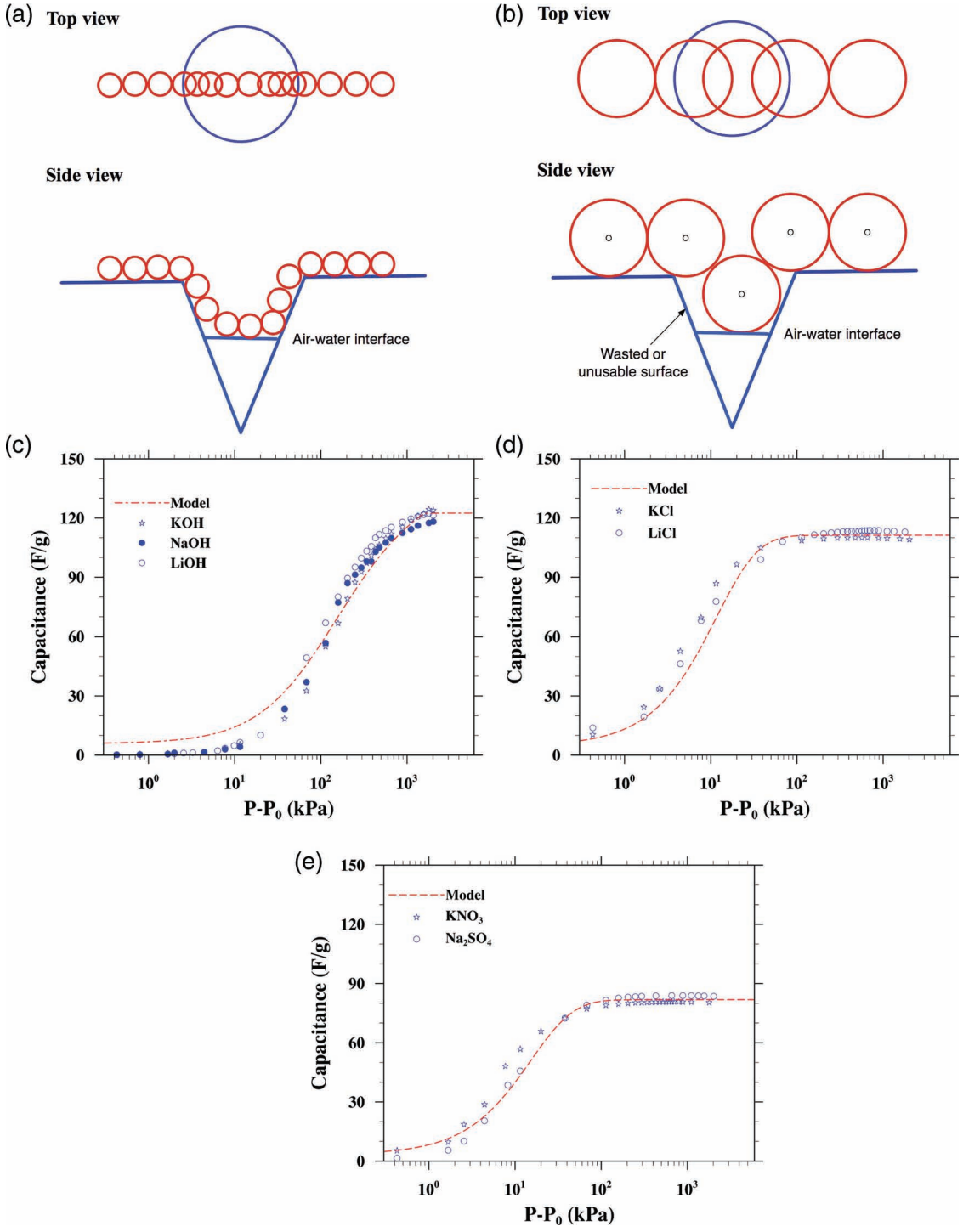

Figure 4. Conceptual approach of the analytical model and comparison of its predicted capacitance with experimental data. a,b) Sketches to show the effect of size exclusion and its dependence on the ion size relative to the pore size. c) The capacitance as a function of applied pressure for KOH, NaOH, and LiOH electrolytes. The parameters used for the model are: $d_i = 0.5$ nm, $C_1 = 8.50$, $\gamma = 0.0$. d) The capacitance as a function of applied pressure for KCl and LiCl electrolytes, the parameters used for the model are: $d_i = 0.64$ nm, $C_1 = 10.8$, $\gamma = 8.0$. e) The capacitance as a function of applied pressure for KNO_3 and Na_2SO_4 electrolytes. The parameters used for the model are: $d_i = 0.7$ nm, $C_1 = 9.50$, $\gamma = 6.0$.

pressures. For supercapacitors with hydrated cations and anions much smaller than the pore size of the ACF electrode, the capacitance was found to continuously increase with increasing applied pressure in the range below 2068 kPa, due to the ever-increasing pore-filling efficiency by ions. In supercapacitors with larger hydrated ions of a size comparable to that of the pore size, the capacitance saturated at pressures much lower than 690 kPa, as the maximum

pore-filling efficiency is reached at much lower applied pressures. The simple but novel analytical model explains well the dependence of capacitance on the applied pressure and the ratio of ion size to pore size, providing a predictive tool towards the realization of low-cost, thin-film, flexible/stretchable supercapacitors.

Experimental Section

Activated Carbon Fabric Electrodes: The activated carbon fabric (ACF) was obtained from Challenge Carbon Technology Co, Taiwan. Using a Micromeritics ASAP2010 system, the Brunauer–Emmett–Teller (BET) surface area and pore-size distributions were determined by isothermal nitrogen adsorption at 77 K.

Electrolyte Preparation: The salts KNO_3, KCl, NaOH, KOH, LiCl, KF, KI, KNO_3, and Na_2SO_4 were purchased from Sigma Aldrich. One molar aqueous electrolyte solutions of each salt were prepared by completely dissolving 1 Mol of the salt in 1 L of deionized (DI) water.

Supercapacitor Assembly: A Wattman glass microfiber filter paper was used as a separator between two circular ACF electrodes of 22.2 mm in diameter obtained by an arch punch. As shown in the schematic of SI, Figure S2a, the supercapacitors with each electrolyte were assembled by placing the sandwich structure of ACF–filter paper–ACF in a laminating pouch with Ni foils (McMaster–Carr) as the current collectors, filled in excess electrolyte to thoroughly wet the ACF/separator structure and sealed the pouch with a hot roller press.

Measurements: The pressure between the electrodes of the supercapacitor was carefully varied in a controlled manner from 0 to 2068 kPa with the help of a Carver hydraulic press by placing the supercapacitor in between the parallel plates of the press as shown in the schematic of SI, Figure S2c. At each applied pressure, the electrochemical characterizations, the cyclic voltammetry (CV) and the electrochemical impedance spectroscopy (EIS) in the two-electrode configuration was carried out using an EG&G PARSTAT 2273 potentiostat/galvanostat (Princeton Applied Research). The CV measurements were performed in the range from 0 to 0.6 V at a scan rate of 10 mV s^{-1}. The EIS measurements were done in the frequency range from 100 KHz to 50 mHz. The capacitance was calculated from the integral area of the voltammogram loop according to the equation

$$C = \frac{A_c + A_d}{v \times \Delta V \times m}$$

where A_c and A_d represent the integral charge area and the discharge area, respectively; v is the scan rate in V s^{-1}, ΔV is the potential window, and m is the average mass of one ACF electrode in grams.

Supporting Information

Supporting Information is available from the Wiley Online Library or from the author.

Acknowledgements

BQW is grateful for financial support from NSF CMMI-0824790.

Received: September 7, 2011
Revised: November 3, 2011
Published online: February 13, 2012

[1] F. Garnier, G. Horowitz, X. H. Peng, D. Fichou, *Adv. Mater.* **1990**, *2*, 592.
[2] F. Garbier, R. Hajlaoui, A. Yassar, P. Srivastava, *Science* **1994**, *265*, 1684.
[3] X. M. Lu, Y. N. Xia, *Nat. Nanotechnol.* **2006**, *1*, 163.
[4] D. H. Kim, J. H. Ahn, W. M. Choi, H. S. Kim, T. H. Kim, J. Song, Y. Y. Huang, Z. Liu, C. Lu, J. A. Rogers, *Science* **2008**, *320*, 507.
[5] P. K. H. Ho, D. S. Thomas, R. H. Friend, N. Tessler, *Science* **1999**, *285*, 233.
[6] H. E. A. Huitema, G. H. Gelinck, J. B. P. H. Van der Putten, K. E. Kuijk, C. M. Hart, E. Cantatore, P. T. Herwig, A. J. J. M. Van Breemen, D. M. de Leeuw, *Nature* **2001**, *414*, 599.
[7] H. C. Ko, M. P. Stoykovich, J. Song, V. Malyarchuk, W. M. Choi, C. J. Yu, J. B. Geddes III, J. Xiao, S. Wang, Y. Huang, J. A. Rogers, *Nature* **2008**, *454*, 748.
[8] J. Viventi, D. H. Kim, J. D. Moss, Y. S. Kim, J. A. Blanco, N. Annetta, A. Hicks, J. Xiao, Y. Huang, D. J. Callans, J. A. Rogers, B. Litt, *Sci. Transl. Med.* **2010**, *2*, 24ra22.
[9] W. Sugimoto, K. Yokoshima, K. Ohuchi, Y. Murakami, Y. Takasu, *J. Electrochem. Soc.* **2006**, *153*, A255.
[10] V. L. Pushparaj, M. M. Shaijumon, A. Kumar, S. Murugesan, L. Ci, R. Vajtai, R. J. Linhardt, O. Nalamasu, P. M. Ajayan, *Proc. Natl. Acad. Sci. USA* **2007**, *104*, 13574.
[11] M. Kaempgen, C. K. Chan, J. Ma, Y. Chi, G. Gruner, *Nano Lett.* **2009**, *9*, 1872.
[12] P. C. Chen, S. G. S. Sukcharoenchoke, C. Zhou, *Appl. Phys. Lett.* **2009**, *94*, 043113.
[13] C. J. Yu, C. Masarapu, J. Rong, B. Q. Wei, H. Jiang, *Adv. Mater.* **2009**, *21*, 4793.
[14] L. B. Hu, M. Pasta, F. L. Mantia, L. F. Cui, S. Jeong, H. D. Deshazer, J. W. Choi, S. M. Han, Y. Cui, *Nano Lett.* **2010**, *10*, 708.
[15] J. Koresh, A. J. Soffer, *J. Electrochem. Soc.* **1977**, *124*, 1379.
[16] C. Largeot, C. Portet, J. Chmiola, P. L. Taberna, Y. Gogotsi, P. Simon, *J. Am. Chem. Soc.* **2008**, *130*, 2730.
[17] R. Lin, P. L. Taberna, J. Chmiola, D. Guay, Y. Gogotsi, P. Simon, *J. Electrochem. Soc.* **2009**, *156*, A7.
[18] J. Chmiola, *Science* **2006**, *313*, 1760.
[19] J. Chmiola, C. Largeot, P. L. Taberna, P. Simon, Y. Gogotsi, *Angew. Chem. Int. Ed.* **2008**, *47*, 3392.
[20] R. A. Howe, W. S. Howells, A. K. Soper, *Nature* **1980**, *287*, 714.
[21] R. Caminiti, G. Licheri, G. Piccaluga, G. Pinna, *J. Chem. Phys.* **1978**, *68*, 1967.
[22] V. Vchirawongkwin, B. M. Rode, I. Persson, *J. Phys. Chem. B* **2007**, *111*, 4150.
[23] A. Kumar, M. Park, J. Y. Huh, H. M. Lee, K. S. Kim, *J. Phys. Chem. A* **2006**, *110*, 12484.
[24] S. B. Rempe, L. R. Pratt, G. Hummer, J. D. Kress, R. L. Martin, A. Redondo, *J. Am. Chem. Soc.* **2000**, *122*, 966.
[25] P. Nicholls, *Cell. Mol. Life Sci.* **2000**, *57*, 987.
[26] K. H. An, W. S. Kim, Y. S. Park, J. M. Moon, D. J. Bae, S. C. Lim, Y. S. Lee, Y. H. Lee, *Adv. Funct. Mater.* **2001**, *11*, 387.
[27] L. P. Wang, B. Q. Wei, unpublished.